Circuit-Based Electrothermal Simulation of Power Devices by an Ultrafast Nonlinear MOR Approach

Lorenzo Codecasa, *Member, IEEE*, Vincenzo d'Alessandro, Alessandro Magnani, *Student Member, IEEE*, and Andrea Irace, *Senior Member, IEEE*

***Abstract*—This paper presents an efficient circuit-based approach for the nonlinear dynamic electrothermal simulation of power devices and systems subject to radical self-heating. The strategy relies on the synthesis of a nonlinear compact thermal network extracted from a finite-element model by a novel model-order reduction method requiring a computational time orders of magnitude lower than conventional techniques. Unlike commonly employed approaches, the proposed network allows reconstructing the whole time evolution of the temperature field in all the points of the domain with high accuracy. Electrothermal simulations are enabled in a commercial SPICE-like simulator by coupling such a network with subcircuits that describe the electrical device behavior by accounting for the temperature dependence of the key physical parameters. As a case study, the dynamic electrothermal analysis of a packaged silicon carbide power MOSFET undergoing a short-circuit test is performed, showcasing the performance of the approach and highlighting the need of including the thermal nonlinearities to achieve reliable results.**

***Index Terms*—Model-order reduction (MOR), nonlinear compact thermal network (NCTN), nonlinear thermal effects, short-circuit test, silicon carbide (SiC) MOSFET.**

I. Introduction

In most applications, power devices and systems are subject to significant self-heating effects, which must be accurately investigated since they may entail a distortion of the characteristics and affect the transistor reliability.

A plethora of methods have been developed over the last decades to perform electrothermal (ET) simulations. Commonly employed approaches involve the interaction between a circuit simulator and a numerical thermal-only tool in a relaxation cycle [1]–[3], or the extension of a finite-element method (FEM) thermal solver to account for the electrical behavior of the transistors with simplified models [4]. However, these strategies are computationally prohibitive and numerically challenging in terms of convergence when geometrically complex domains requiring fine meshes are to be analyzed. Another method relies on the coupling inside a circuit solver of 1) subcircuits that describe the electrical device behavior by including the temperature dependence of the key physical parameters, and 2) a thermal network (i.e., an equivalent circuit) that accounts for the heat diffusion within the structure, and can be derived from the equations discretizing the heat diffusion with numerical techniques such as the FEM [5]–[12]; in this case, the CPU/memory burden can be alleviated by substituting the large thermal networks needed for modern power devices with *compact* thermal networks (CTNs), in principle having dimensions comparable to those of the electrical circuit.

Various methods exist for constructing CTNs modeling heat diffusion in dynamic *linear* conditions, when all thermal parameters can be assumed to be temperature insensitive; especially effective are the model-order reduction (MOR) techniques and in particular the multipoint moment matching (MPMM) algorithm [13]–[17]. However, it has been shown that including the effects of temperature-dependent thermal conductivities (*nonlinear* thermal effects) in CTNs is crucial in power electronics [18]. The most commonly adopted approach (due to its simple application) is based on the Kirchhoff's transformation [7], [19], [20], by which CTNs extracted assuming temperature-independent thermal conductivities are extended to the nonlinear case. Unfortunately, this procedure in practice provides exact results only under steady-state conditions and considering a single material for the entire device, while introducing large inaccuracies in practical cases, as investigated by the Authors in [21]. Some attempts for a more accurate description of nonlinear thermal effects in power devices can be encountered in the recent literature. Methods using nonlinear thermal networks directly obtained by discretizing the heat diffusion equations are reported in [22] and [23]; these works propose strategies for managing the large computational complexity of ET simulations when directly using thermal circuits derived by discretization. Following [18], nonlinear CTNs (NCTNs) with Cauer topology have been conceived: in [24], a network with power-dependent resistors and capacitors is determined by fitting with thermal impedances measured in the time domain for various power levels; in [25], a network with temperature-dependent resistors is generated through a physics-based procedure verified by comparison with 3-D numerical results. Another strategy for constructing geometry-scalable NCTNs involves the use of simplifying assumptions on the heat propagation in the specific domain under analysis, as performed in [26] for trench-isolated heterojunction bipolar transistors.

In this paper, an alternative approach is proposed, which allows performing extremely fast, yet accurate, nonlinear ET analyses of power transistors for any level of temperature by representing the whole structure under analysis with a single

Manuscript received June 30, 2015; revised September 2, 2015; accepted October 8, 2015. Date of publication October 26, 2015; date of current version March 2, 2016. Recommended for publication by Associate Editor A. Lindemann.

L. Codecasa is with the Department of Electronics, Information and Bioengineering, Politecnico di Milano, Milan 20133 Italy (e-mail: lorenzo.codecasa@polimi.it).

V. d'Alessandro, A. Magnani, and A. Irace are with the Department of Electrical Engineering and Information Technology, University Federico II, 80125 Naples, Italy (e-mail: vindales@unina.it; alessandro.magnani@unina.it; andrea.irace@unina.it).

electrical macrocircuit making use of transistor subcircuits that include temperature-dependent parameters, and a novel highly efficient NCTN to describe the power-temperature feedback; as a result, nonlinear ET simulations can be performed by resorting to the optimized engines of commercial SPICE-like circuit simulators.

The NCTN is obtained by extending the nonlinear MOR technique proposed in [21] so as to cover a much wider range of temperature; thus, accuracy is ensured in describing power devices operated under extremely harsh conditions (e.g., energy distribution, automotive, railway traction, aircraft, and spacecraft applications), for which a conventional linear ET analysis would provide an unacceptable underestimation of thermal issues. The resulting method, differently from previous techniques, does not need cumbersome measurements, costly 3-D numerical transient simulations of discretized nonlinear heat diffusion equations, or simplifying assumptions on the geometry of the domain, and can be effortlessly applied to any device category, including packages, for any input power profile (even for short huge-power pulses). Moreover, such an NCTN allows determining the temperature field in the whole structure under analysis (i.e., in all points of the computational domain) in a postprocessing step.

The remainder of this paper is articulated as follows. In Sections II–IV, details are given on the analytical derivation of the nonlinear MOR technique, as well as of the NCTN. In Section V, the proposed approach is exploited to examine the nonlinear thermal and ET behavior of a packaged silicon carbide (SiC) power MOSFET suffering from high temperature induced by hard short-circuit conditions. Conclusions are then drawn in Section VI. In the Appendix, the Kirchhoff's trasformation approach, used throughout the paper for comparison, is reported.

II. Reformulation of the Nonlinear Heat Diffusion Problem

A nonlinear heat diffusion problem, in the spatial domain Ω, is ruled by equation

$$\rho(\mathbf{r})c(\mathbf{r})\frac{\partial \vartheta}{\partial t}(\mathbf{r},t)+\nabla\cdot[-k(\mathbf{r},\vartheta(\mathbf{r},t))\nabla\vartheta(\mathbf{r},t)]=q(\mathbf{r},t) \quad (1)$$

in which $\vartheta(\mathbf{r},t)$ is the temperature rise with respect to ambient temperature $T_0 = 300$ K due to the power density $q(\mathbf{r},t)$, $\mathbf{r}$ and t being the position vector and the time instant, respectively. The specific heat $c(\mathbf{r})$ and the mass density $\rho(\mathbf{r})$ can be assumed as temperature insensitive. However, the dependence of thermal conductivity on $\vartheta(\mathbf{r},t)$ cannot be disregarded and is thus taken into account in the form

$$k(\mathbf{r},\vartheta(\mathbf{r},t))=k_0(\mathbf{r})\left(1+\frac{\vartheta(\mathbf{r},t)}{T_0}\right)^{m(\mathbf{r})} \quad (2)$$

in which parameters $k_0(\mathbf{r})$ and $m(\mathbf{r})$ have different values in different materials. Robin conditions can be assumed on the boundary $\partial\Omega$ of Ω, in the form

$$-k(\mathbf{r},\vartheta(\mathbf{r},t))\frac{\partial \vartheta}{\partial n}(\mathbf{r},t)=h(\mathbf{r})\vartheta(\mathbf{r},t) \quad (3)$$

in which $\mathbf{n}(\mathbf{r})$ is the outward normal unit vector, and $h(\mathbf{r})$ is the heat transfer coefficient, which is generally assumed to be temperature independent. Due to the difficulty in estimating the heat transfer coefficients, often either Neumann or Dirichlet boundary conditions are preferred, which can be obtained from (3) taking the limits $h(\mathbf{r}) \to 0$ and $h(\mathbf{r}) \to \infty$, respectively. Homogeneous initial conditions can be considered, i.e., $\vartheta(\mathbf{r},0) = 0$ K.

In view of the construction of the NCTNs, the nonlinear heat diffusion problem is reformulated in an *equivalent* way in which only quadratic nonlinearities occur. More specifically, by introducing the additional variable

$$\lambda(\mathbf{r},t)=\left(1+\frac{\vartheta(\mathbf{r},t)}{T_0}\right)^{m(\mathbf{r})}-1 \quad (4)$$

(1) and (3) are rewritten in the form

$$\rho(\mathbf{r})c(\mathbf{r})\frac{\partial \vartheta}{\partial t}(\mathbf{r},t)+\nabla\cdot[-k_0(\mathbf{r})(1+\lambda(\mathbf{r},t))\nabla\vartheta(\mathbf{r},t)] = g(\mathbf{r})P(t), \quad (5)$$

$$-k_0(\mathbf{r})(1+\lambda(\mathbf{r},t))\frac{\partial \vartheta}{\partial n}(\mathbf{r},t)=h(\mathbf{r})\vartheta(\mathbf{r},t). \quad (6)$$

Besides, by deriving (4) with respect to time, it is obtained

$$(T_0+\vartheta(\mathbf{r},t))\frac{\partial \lambda}{\partial t}(\mathbf{r},t)=m(\mathbf{r})(1+\lambda(\mathbf{r},t))\,\frac{\partial \vartheta}{\partial t}(\mathbf{r},t). \quad (7)$$

Equation (7) is *equivalent* to (4), assuming initial condition $\lambda(\mathbf{r},0)=0$.

A thermal model is defined by introducing its port variables [16], allowing the coupling of electric circuits to NCTNs for ET simulations. Thus, for the case here considered, the power density $q(\mathbf{r},t)$ is written in the form

$$q(\mathbf{r},t)=g(\mathbf{r})P(t) \quad (8)$$

in which $P(t)$ is the power dissipated by the active heat source and injected at the port of the NCTN, while

$$\Delta T(t)=\int_\Omega g(\mathbf{r})\vartheta(\mathbf{r},t)\,d\mathbf{r} \quad (9)$$

defines the average temperature rise over the active heat source, which can be measured at the port of the NCTN.

III. Nonlinear Compact Thermal Network

The NCTN is here achieved from the nonlinear heat diffusion equations, as reformulated in Section II, by an MOR approach that preserves their nonlinear quadratic structure. To this aim, $\vartheta(\mathbf{r},t)$ is approximated in the form

$$\vartheta(\mathbf{r},t)=\sum_{j=1}^{\hat{n}_\vartheta}\vartheta_j(\mathbf{r})\,\hat{\vartheta}_j(t) \quad (10)$$

in which $\vartheta_j(\mathbf{r})$ are a small number $\hat{n}_\vartheta$ of orthonormal basis functions, which will be determined in Section IV. Likewise $\lambda(\mathbf{r},t)$ is approximated in the form

$$\lambda(\mathbf{r},t)=\sum_{s=1}^{\hat{n}_\lambda}\lambda_s(\mathbf{r})\,\hat{\lambda}_s(t) \quad (11)$$

in which $\lambda_s(\mathbf{r})$ are a small number $\hat{n}_\lambda$ of orthonormal basis functions, which again will be determined in Section IV.

By multiplying (5) by $\vartheta_i(\mathbf{r})$, integrating over Ω, applying the divergence theorem and recalling (6), (10), and (11), the following equations are obtained for all $i = 1, \ldots, n_\vartheta$:

$$\frac{d\hat{\vartheta}_i}{dt}(t) + \sum_{j=1}^{\hat{n}_\vartheta} \left(\hat{K}_{ij}^0 + \sum_{s=1}^{\hat{n}_\lambda} \hat{K}_{ij}^s \hat{\lambda}_s(t) \right) \hat{\vartheta}_j(t) = \hat{g}_i P(t) \quad (12)$$

in which

$$\begin{aligned} \hat{K}_{ij}^0 &= \int_\Omega k_0(\mathbf{r}) \nabla\vartheta_i(\mathbf{r}) \cdot \nabla\vartheta_j(\mathbf{r})\, d\mathbf{r} + \int_{\partial\Omega} h(\mathbf{r})\vartheta_i(\mathbf{r})\vartheta_j(\mathbf{r})\, d\mathbf{r} \\ \hat{K}_{ij}^s &= \int_\Omega k_0(\mathbf{r}) \nabla\vartheta_i(\mathbf{r}) \cdot \nabla\vartheta_j(\mathbf{r}) \lambda_s(\mathbf{r})\, d\mathbf{r} \\ \hat{g}_i &= \int_\Omega g(\mathbf{r})\vartheta_i(\mathbf{r})\, d\mathbf{r}. \end{aligned} \quad (13)$$

Similarly, multiplying (7) by $\lambda_r(\mathbf{r})$, integrating over Ω and recalling (10), (11), it is found for all $r = 1, \ldots, n_\lambda$

$$\begin{aligned} &\sum_{s=1}^{\hat{n}_\lambda} \left(T_0\, \delta_{rs} + \sum_{j=1}^{\hat{n}_\vartheta} \hat{C}_{rs}^j \hat{\vartheta}_j(t) \right) \frac{d\hat{\lambda}_s}{dt}(t) \\ &+ \sum_{j=1}^{\hat{n}_\lambda} \left(\sum_{k=1}^{\hat{n}_\vartheta} \hat{G}_{rs}^j \hat{\varphi}_j(t) \right) \hat{\lambda}_s(t) = \sum_{j=1}^{\hat{n}_\vartheta} \hat{f}_r^j \hat{\varphi}_j(t) \end{aligned} \quad (14)$$

in which δ is the Kronecker's delta symbol, $\hat{\varphi}_j(t) = d\hat{\vartheta}_j/dt(t)$ and

$$\begin{aligned} \hat{C}_{rs}^j &= \int_\Omega \lambda_r(\mathbf{r})\lambda_s(\mathbf{r})\vartheta_j(\mathbf{r})\, d\mathbf{r} \\ \hat{G}_{rs}^j &= \int_\Omega m(\mathbf{r})\lambda_r(\mathbf{r})\lambda_s(\mathbf{r})\vartheta_j(\mathbf{r})\, d\mathbf{r} \\ \hat{f}_r^j &= \int_\Omega m(\mathbf{r})\lambda_r(\mathbf{r})\vartheta_j(\mathbf{r})\, d\mathbf{r}. \end{aligned}$$

From the initial conditions of the nonlinear heat diffusion problems ensue $\hat{\vartheta}_i(t) = 0$, $\hat{\lambda}_r(t) = 0$. Equations (12) and (14) define a nonlinear thermal model that allows approximating the average temperature rise over the heat source in the form

$$\Delta T(t) = \sum_{j=1}^{\hat{n}_\vartheta} \hat{g}_j \hat{\vartheta}_j(t) \quad (15)$$

in which $\hat{g}_i$ are defined by (13). Moreover such nonlinear thermal model, in a postprocessing stage, allows reconstructing the whole temperature rise evolution $\vartheta(\mathbf{r}, t)$ within Ω by (10).

Equations (12), (14), and (15) can be interpreted as the Nodal Analysis equations of the NCTN shown in Fig. 1. In particular, (12) models subcircuit $\mathcal{N}_\vartheta$ made of n_ϑ nodes at which potentials $\hat{\vartheta}_i(t)$ are measured. The first term on the left-hand side of (12) models n_ϑ capacitors of unit capacitance connecting each node i of $\mathcal{N}_\vartheta$ to ground; the second term models $n_\vartheta(n_\vartheta + 1)/2$ resistors connecting each pair of nodes $i \neq j$ of $\mathcal{N}_\vartheta$ and each node i of $\mathcal{N}_\vartheta$ to ground, and having conductances

$$\hat{k}_{ij}^0 + \sum_{s=1}^{\hat{n}_\lambda} \hat{k}_{ij}^s \hat{\lambda}_s(t)$$

in which

$$\hat{k}_{ii}^s = \sum_{j=1}^{n_\vartheta} \hat{K}_{ij}^s, \quad \hat{k}_{ij}^s = -\hat{K}_{ij}^s \text{ for } i \neq j.$$

Such conductances linearly depend on the potentials $\hat{\lambda}_i(t)$ of subcircuit $\mathcal{N}_\lambda$, defined below. The right-hand side of (12) models n_ϑ current sources controlled by power $P(t)$.

Analogously, (14) models subcircuit $\mathcal{N}_\lambda$ of the NCTN shown in Fig. 1 made of n_λ nodes at which potentials $\hat{\lambda}_r(t)$ are measured. The first term in the left-hand side of (14) models $n_\lambda(n_\lambda + 1)/2$ capacitors connecting each pair of nodes $r \neq s$ of $\mathcal{N}_\lambda$ and each node r of $\mathcal{N}_\lambda$ to ground, and having capacitances

$$T_0 \delta_{rs} + \sum_{j=1}^{\hat{n}_\vartheta} \hat{c}_{rs}^j \hat{\vartheta}_j(t)$$

in which

$$\hat{c}_{rr}^j = \sum_{s=1}^{n_\lambda} \hat{C}_{rs}^j, \quad \hat{c}_{rs}^j = -\hat{C}_{rs}^j \text{ for } r \neq s.$$

Such capacitances linearly depend on the potentials $\hat{\vartheta}_i(t)$ of subcircuit $\mathcal{N}_\vartheta$. The second term models $n_\lambda(n_\lambda + 1)/2$ resistors connecting each pair of nodes $r \neq s$ of $\mathcal{N}_\lambda$ and each node r of $\mathcal{N}_\lambda$ to ground, and having conductances

$$\sum_{j=1}^{\hat{n}_\vartheta} \hat{g}_{rs}^j \hat{\varphi}_j(t)$$

in which

$$\hat{g}_{rr}^j = \sum_{s=1}^{n_\lambda} \hat{G}_{rs}^j, \quad \hat{g}_{rs}^j = -\hat{G}_{rs}^j \text{ for } r \neq s.$$

Such conductances linearly depend on the variables $\hat{\varphi}_i(t)$ of subcircuit $\mathcal{N}_\vartheta$. The right-hand side of (14) models n_λ current sources controlled by the variables $\hat{\varphi}_i(t)$ of subcircuit $\mathcal{N}_\vartheta$.

Equation (15) models subcircuit $\mathcal{N}_T$ of the NCTN shown in Fig. 1 having one node in addition to the thermal node of the power device and including a current source controlled by the potentials $\hat{\vartheta}_i(t)$ of subcircuit $\mathcal{N}_\vartheta$.

The voltage-controlled resistors and capacitors can be implemented in SPICE-like circuit environments, as reported in [27].

IV. Basis functions from Volterra's Kernels

In order to determine the basis functions $\vartheta_j(\mathbf{r})$, and $\lambda_j(\mathbf{r})$, the m-order Volterra's kernels [28] of $\vartheta(\mathbf{r}, t)$ and $\lambda(\mathbf{r}, t)$, named $\Theta_m(\mathbf{r}, \boldsymbol{\sigma}_m)$, $\Lambda_m(\mathbf{r}, \boldsymbol{\sigma}_m)$, are evaluated at a few $m \times 1$ frequency vectors $\boldsymbol{\sigma}_m$, for $m = 1, \ldots, M$, with a chosen small M, using an extended version of the method presented in [21], as detailed hereinafter.

The Volterra's kernels $\Theta_m(\mathbf{r}, \boldsymbol{\sigma}_m)$ are computed by iteratively solving from $m = 1$ to $m = M$ the *linear* heat diffusion

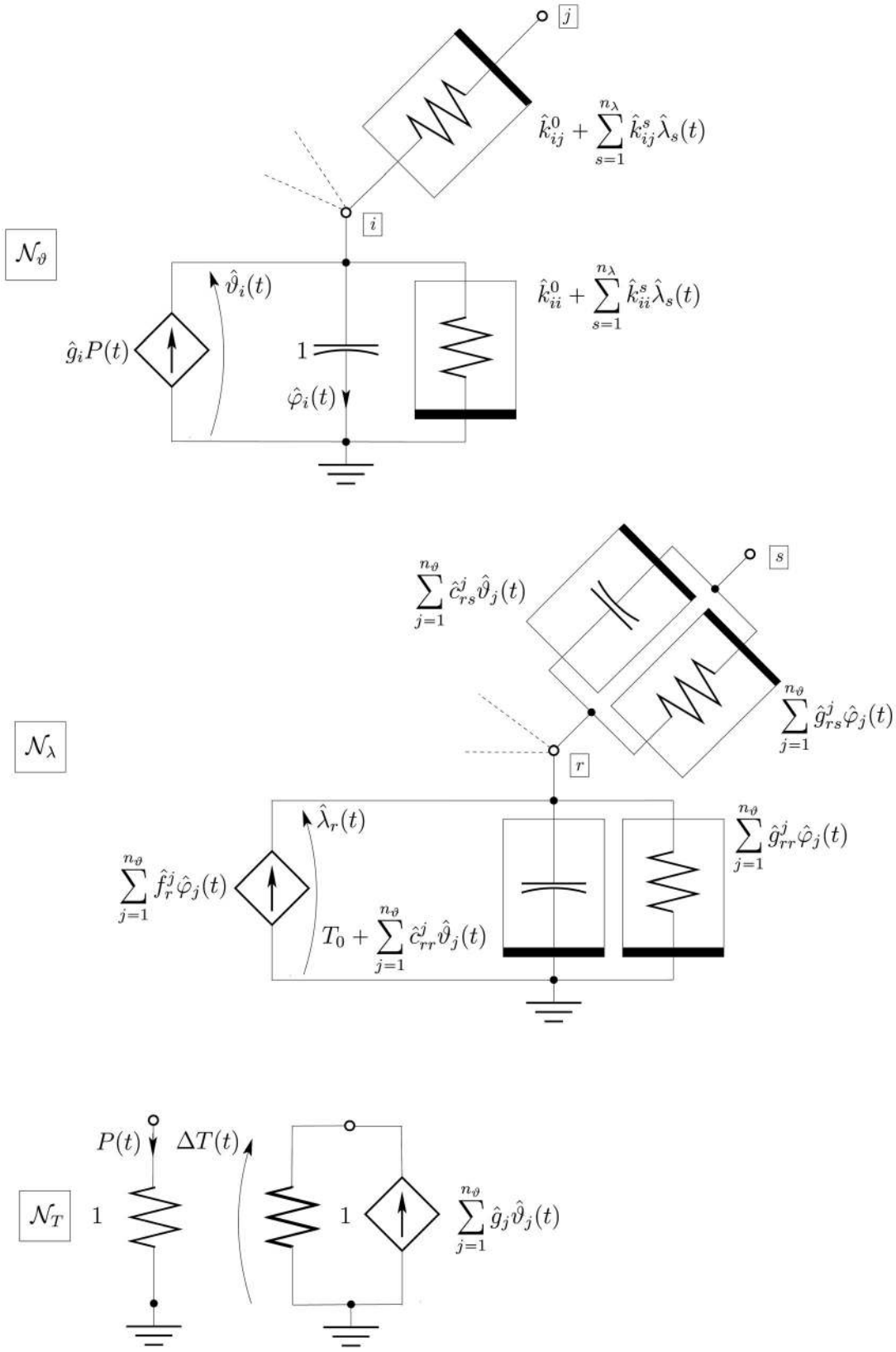

Fig. 1. Proposed NCTN topology composed of subcircuits $\mathcal{N}_\vartheta$, $\mathcal{N}_\lambda$, $\mathcal{N}_T$. Conductances and capacitances are indicated for resistors and capacitors, respectively.

problem in the frequency domain given by (16) with boundary conditions over $\partial\Omega$ (17), in which the right-hand side is known from previous iterations. In these expressions, $\boldsymbol{p}_m$ is a vector of m elements equal to either zero or one, $|\boldsymbol{p}_m|$ indicates the sum of the elements of $\boldsymbol{p}_m$, and $\boldsymbol{p}'_m$ is the vector obtained from $\boldsymbol{p}_m$ by exchanging all zeros with ones and ones with zeros. Moreover, $\boldsymbol{\sigma}_m^{\boldsymbol{p}_m}$ is the vector obtained by selecting the elements of $\boldsymbol{\sigma}_m$ corresponding to the ones of $\boldsymbol{p}_m$, see equations (16), (17) and (18) shown at the bottom of the page.

The Volterra's kernels $\Lambda_{m,\boldsymbol{\alpha}_m}(\mathbf{r},\boldsymbol{\sigma}_m) = \Omega_m(\mathbf{r},\boldsymbol{\sigma}_m)/|\boldsymbol{\sigma}_m|$ are iteratively determined from $m=1$ to $m=M$ by (18), in which $\Phi_m(\mathbf{r},\boldsymbol{\sigma}_m) = |\boldsymbol{\sigma}_m|\,\Theta_m(\mathbf{r},\boldsymbol{\sigma}_m)$.

Orthonormal basis functions $\vartheta_j(\mathbf{r})$ and $\lambda_j(\mathbf{r})$ spanning the computed moments $\Theta_m(\mathbf{r},\boldsymbol{\sigma}_m)$ and $\Lambda_m(\mathbf{r},\boldsymbol{\sigma}_m)$, respectively, are then obtained by singular value decomposition (SVD).

The set of frequency vectors $\boldsymbol{\sigma}_m$ can be chosen in many different ways. A simple choice is made in the following, which extends what is usual in MPMM for linear heat diffusion problems [12]. The set of N positive real frequencies $\beta_1 < \beta_2 < \ldots \beta_N$ introduced in MPMM is considered. These are used to define vectors

$$\boldsymbol{\sigma}_m = \overbrace{(\beta_i, \beta_1, \ldots, \beta_1)}^{m}, \quad i = 1, \ldots, N, \quad m = 1, \ldots, M.$$

As shown in the numerical section, this choice of frequency vectors allows getting accurate NCTNs up to extreme levels of temperature for all waveforms of dissipated power of practical interest.

Hence, a set of $M \cdot N$ linear heat diffusion problems in the frequency domain is to be numerically solved. The computational complexity of the whole approach is almost entirely due to the solution to these problems, which is performed over a tetrahedral mesh by 2nd-order FEM spatial approximation of the temperature rise. The resulting linear systems of equations are solved by an efficient algebraic multigrid iterative solver [29].

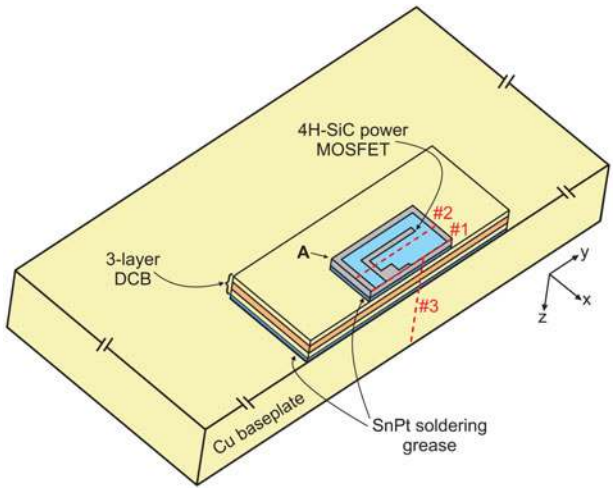

Fig. 2. 3-D representation of the structure under test; point A is the origin of the system of coordinates.

V. Case Study

A. Device Under Test

The proposed NCTN was adopted to investigate both the thermal and ET behavior of a 1200-V 50-A 4H-SiC power MOSFET manufactured by CREE [30] and bonded to a widely used direct copper bonding (DCB) package (e.g., [31]). The analysis is of utmost interest since—in spite of the well-known superior performance of SiC power devices in terms of thermal conductivity [32]—SiC MOSFETs might experience a detrimentally high positive temperature coefficient (PTC) of the drain current induced by traps located at the SiO_2/SiC, as detailed later.

A 3-D representation of the structure under test is depicted in Fig. 2. The active area of the 0.4 cm $\times$0.4 cm 370-μm-thick bare die is covered by a 4-μm-thick Al source metallization. The two-layer (0.8-μm-thick Ni and 0.6-μm-thick Ag) backside drain contact is attached through a 200-μm-thick SnPt soldering grease to an 0.8 cm $\times$1 cm DCB substrate comprising three layers, namely, 0.3-mm-thick Cu, 0.38-mm-thick Al_2O_3, and 0.3-mm-thick Cu. The DCB is in turn soldered with a SnPt

$$|\boldsymbol{\sigma}_m|\,\rho(\mathbf{r})c(\mathbf{r})\Theta_m(\mathbf{r},\boldsymbol{\sigma}_m) + \nabla\cdot(-k_0(\mathbf{r})\nabla\Theta_m(\mathbf{r},\boldsymbol{\sigma}_m))$$
$$= -\sum_{k=1}^{m-1}\nabla\cdot\left(-k_0(\mathbf{r})\sum_{|\boldsymbol{p}_m|=k}\Lambda_k(\mathbf{r},\boldsymbol{\sigma}_m^{\boldsymbol{p}_m})\nabla\Theta_{m-k}(\mathbf{r},\boldsymbol{\sigma}_m^{\boldsymbol{p}'_m})\right)\Bigg/\binom{m}{k} + g(\mathbf{r})\delta_{m1} \tag{16}$$

$$-k_0(\mathbf{r})\frac{\partial\Theta_m}{\partial n}(\mathbf{r},\boldsymbol{\sigma}_m) - h(\mathbf{r})\Theta_m(\mathbf{r},\boldsymbol{\sigma}_m) = -\sum_{k=1}^{m-1}k_0(\mathbf{r})\sum_{|\boldsymbol{p}_m|=k}\Lambda_k(\mathbf{r},\boldsymbol{\sigma}_m^{\boldsymbol{p}_m})\frac{\partial\Theta_{m-k}}{\partial n}(\mathbf{r},\boldsymbol{\sigma}_m^{\boldsymbol{p}'_m})\Bigg/\binom{m}{k} \tag{17}$$

$$\Omega_m(\mathbf{r},\boldsymbol{\sigma}_m) = -\sum_{k=1}^{m-1}\sum_{|\boldsymbol{p}_m|=k}\Theta_k(\mathbf{r},\boldsymbol{\sigma}_m^{\boldsymbol{p}_m})\Omega_{m-k}(\mathbf{r},\boldsymbol{\sigma}_m^{\boldsymbol{p}'_m})\Bigg/\binom{m}{k}$$
$$+ m(\mathbf{r})\left(\Phi_m(\mathbf{r},\boldsymbol{\sigma}_m) + \sum_{k=1}^{m-1}\sum_{|\boldsymbol{p}_m|=k}\Lambda_k(\mathbf{r},\boldsymbol{\sigma}_m^{\boldsymbol{p}_m})\Phi_{m-k}(\mathbf{r},\boldsymbol{\sigma}_m^{\boldsymbol{p}'_m})\Bigg/\binom{m}{k}\right) \tag{18}$$

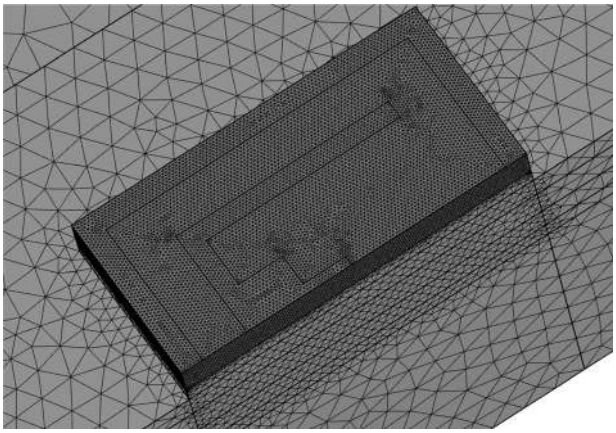

Fig. 3. Detail of the Comsol grid used for the 3-D FEM simulations.

TABLE I
MATERIAL PARAMETERS USED FOR THE THERMAL SIMULATIONS

Material	k at T_0 [W/mK]	ρ [kg/m^3]	c [J/kgK]	m
4H-SiC	370 [34]	3211	690	−1.29 [35]
Al	200	2700	900	0
SnPt	50	7310	228	0
Ni	90.5	8908	444	−0.44 [36]
Ag	429	10490	235	0
Poly	40	2330	920	0
SiO_2	1.33	2203	709	0.33 [37]
Al_2O_3	28	3900	796	−1 [37]
Cu	398	8900	385	0

grease to a 3-mm-thick 4 cm ×4 cm Cu baseplate mounted onto an aluminum heat sink.

B. Thermal Analysis

Half of the structure under test was drawn within the environment of the FEM software package Comsol [33] for thermal-only simulations. The meshing process was supported by the advanced features for selective refinement available in the tool; the resulting grid, a detail of which is reported in Fig. 3, involves 1.1×10^6 tetrahedra and 1.5×10^6 degrees of freedom. The missing portion was virtually restored by applying an adiabatic boundary condition over the plane of symmetry.

The bottom of the Cu baseplate was supposed to be in intimate contact with an ideal heat sink kept at the reference temperature T_0. All other surfaces were reasonably assumed adiabatic. The active device area (i.e., the region including the elementary channels) was modeled with one thin heat source.

All material parameters used for the thermal simulations (namely, thermal conductivity k, mass density ρ, and specific heat c) were chosen according to data reported in the literature, and are listed in Table I. The temperature dependence of k was enabled for 4H-SiC, Ni, SiO_2, and Al_2O_3 according to the power law (2), whereas it was safely disregarded for other materials; it can be evinced that such dependence is highly nonuniform in the structure: k collapses with increasing temperature in 4H-SiC, while being almost temperature-insensitive within the whole package.

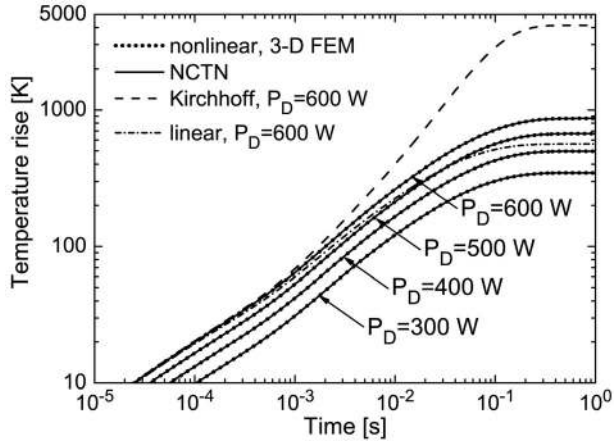

Fig. 4. Transient evolution of the nonlinear temperature rise over ambient corresponding to various P_D steps, as obtained by making use of the proposed NCTN (solid lines) and 3-D Comsol simulations (dotted); also shown are the curves determined for the case $P_D = 600$ W by deactivating the temperature dependence of the thermal conductivities (dot-dashed) and applying the Kirchhoff's transformation (dashed).

The overall analysis was executed on a PC equipped with 32-GB RAM and a quad-core i7-3820QM. The proposed NCTN with $n_\vartheta = n_\lambda = 41$ was extracted from the Comsol grid in about 2 h by exploiting the procedure presented in Sections II–IV with $M = 7$ and $N = 10$. It is noteworthy that increasing M from 4 (as considered in [21]) to 7, the maximum temperature rise for which the NCTN exhibits 0.1% accuracy extends from about 400 to 1000 K. Nonlinear transient thermal simulations up to steady-state conditions were performed by applying power steps with amplitude spanning from 300 to 600 W. The resulting temperature rises above ambient—evaluated as an average of the temperature field over the heat source—are illustrated in Fig. 4. The following findings are observed:

- the CPU time needed to compute a single curve with the proposed NCTN amounted to 80 s by using the popular PSPICE program [38];
- conversely, a standard 3-D Comsol simulation required more than 20 h;
- excellent agreement is obtained between the results determined with the NCTN and the Comsol counterparts, even for very high temperature values;
- disregarding nonlinear thermal effects leads to a significant temperature underestimation (560 K instead of the exact 865 K under steady-state conditions for $P_D = 600$ W), while a huge overestimation is obtained by applying to the whole domain the Kirchhoff's transformation with the 4H-SiC dependence of k upon temperature (4160 K for the same scenario).

As underlined in Section III, the presented approach allows also reconstructing the entire 3-D temperature field for each time instant. Fig. 5 illustrates some temperature rise profiles along the horizontal cuts indicated as #1 and #2 in Fig. 2, and taken along the plane where the heat source is located. It can be inferred that a perfect match occurs between the results

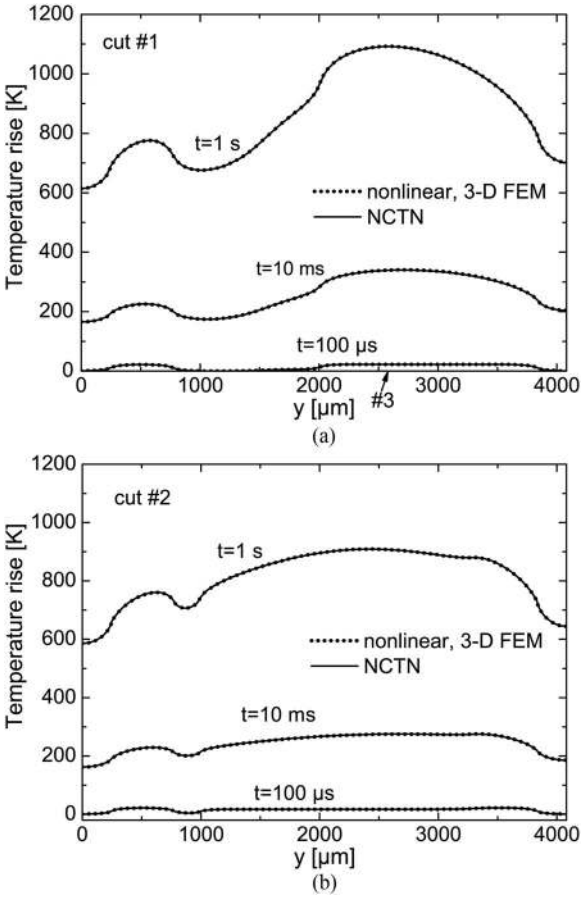

Fig. 5. Temperature rise profiles along the horizontal cuts (a) #1 and (b) #2 illustrated in Fig. 2 for $t = 100$ μs, 10 ms, and 1 s, as computed by the proposed NCTN (solid lines) and Comsol simulations (dotted) for the $P_D = 600$ W step. Also shown in (a) is the abscissa along which the vertical cut #3 is taken.

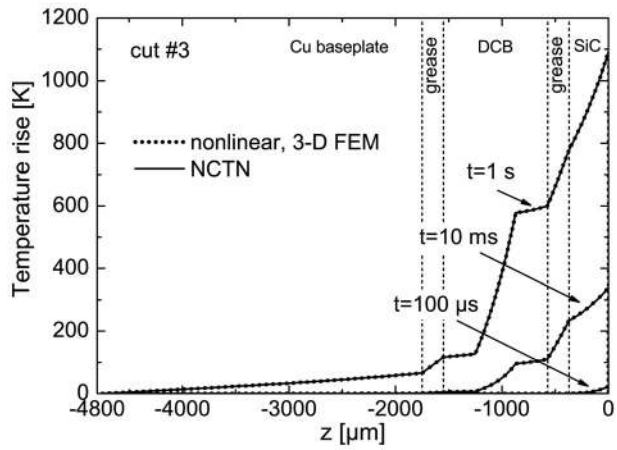

Fig. 6. Temperature rise profiles along the vertical cut #3 evidenced in Fig. 2 for $t = 100$ μs, 10 ms, and 1 s, as evaluated through the proposed NCTN (solid lines) and Comsol simulations (dotted) for the power step with $P_D = 600$ W.

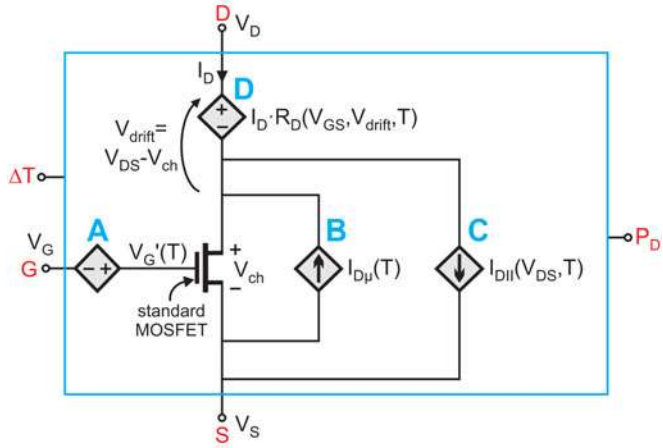

Fig. 7. Sketch of the subcircuit corresponding to the SiC power MOSFET [39].

evaluated with the proposed NCTN and Comsol. The shape of the profiles corresponding to cut #1 is determined by the position of the active areas (i.e., of the heat source); in particular, after a peripheral inactive area (from $y = 0$ to 250 μm), there is a small active region (up to $y = 700$ μm) leading to a temperature "bump," followed by an inactive sector underneath the gate contact (up to $y = 2010$ μm), a large active region, and another inactive area near the die border. Similar considerations can be derived for the curves corresponding to cut #2, where the inactive area associated to the gate contact lies between $y = 770$ and 990 μm.

Fig. 6 reports the temperature rise profiles along the vertical cut referred to as #3 in Fig. 2 for the same time instants as in Fig. 5; a simple inspection of the curves reveals that

- the sharp slope of the temperature within the MOSFET for long times shows that the thermal conductivity of 4H-SiC has noticeably decreased with respect to the T_0 value due to nonlinear thermal effects;
- the low thermally conductive layers of soldering grease and of the DCB dielectric Al_2O_3 severely counteract the downward heat propagation [31], which instead becomes much faster within the Cu layers and the Cu baseplate.

C. Electrical Macromodeling

According to the *macromodeling technique*, the power MOSFET is represented by a subcircuit, which—besides the standard device terminals—is equipped with an input node fed with the temperature rise above ambient and an output node providing the dissipated power. The subcircuit—a simplified schematic of which is shown in Fig. 7—is composed by a standard device component as a main element, as well as resistances and supplementary linear/nonlinear controlled sources to include specific physical mechanisms and to allow the variation of the temperature-sensitive parameters during the simulation run. A slightly improved variant of the transistor model proposed in [39] is implemented, the main features of which can be described as follows.

- The threshold voltage suffers from a negative temperature coefficient (NTC) much higher than that of similarly-rated Si transistors due to the high density of SiO_2/Si interface traps [40]–[42]; this mechanism is accounted for through the voltage source A in series with the gate.

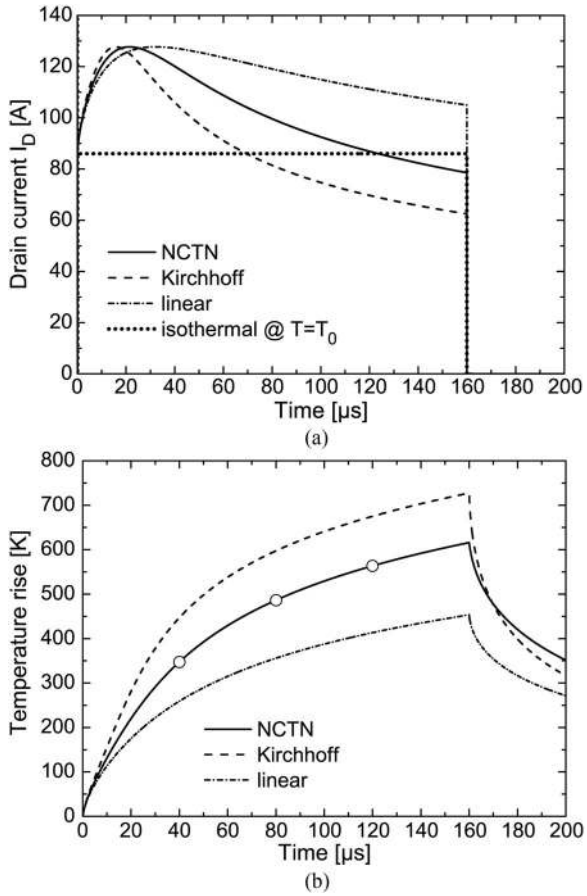

Fig. 8. PSPICE simulations of a short-circuit test performed on the structure under analysis by applying $V_{GS} = 20$ V and $V_{DS} = 100$ V for 160 μs: (a) time evolution of the drain current, as determined under isothermal conditions at $T = T_0$ (dotted line), as well as by activating the ET feedback with a linear CTN (dot-dashed), through the same CTN equipped with an additional generator to account for the Kirchhoff's transformation (dashed), and by exploiting the proposed NCTN (solid); (b) corresponding temperature rises above ambient for all the ET cases. In (b), circles identify the operating points examined in Figs. 9 and 10.

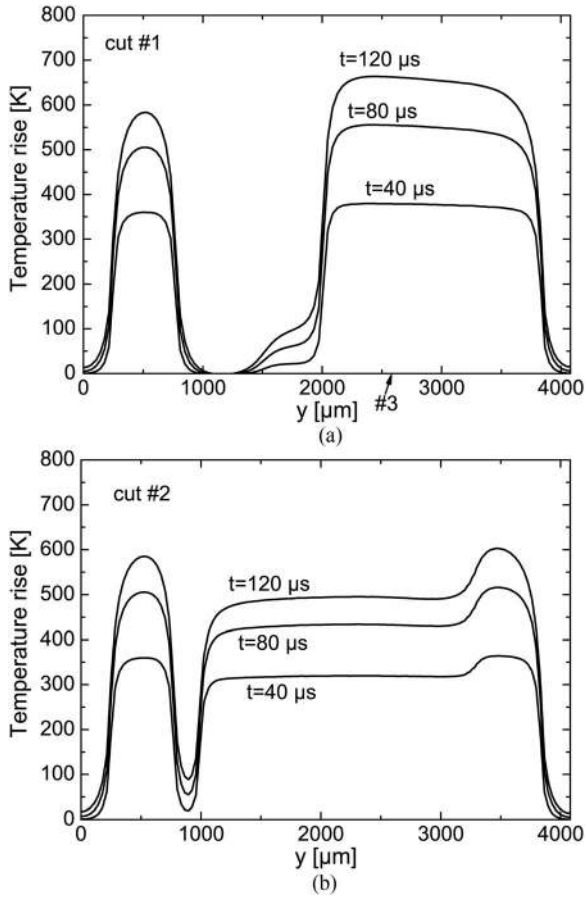

Fig. 9. Temperature rise profiles along the horizontal cuts (a) #1 and (b) #2 illustrated in Fig. 2 during the short-circuit test at $t = 40$, 80, and 120 μs, as computed in a postprocessing step.

- The channel mobility exhibits a PTC at low-medium temperatures absent in Si devices and again attributed to the interface traps, the expected NTC due to the phonon-acoustic scattering being restored at very high temperatures [42]–[45]; this behavior is enabled by placing the current source B in parallel with the standard MOSFET.
- Impact-ionization effects are included by paralleling the current source C to the device enriched with the temperature dependence of both threshold voltage and mobility.
- The drift resistance and its sensitivity to biasing conditions are emulated by the additional voltage source D connected to the drain.

It is worth noting that the concurrent action of the high NTC of threshold voltage and PTC of channel mobility may entail a significant—and thus, harmful—PTC of the drain current at low-medium temperatures that must be properly described by simulation tools.

The model parameters, including the temperature-scaling ones, were calibrated on experimental data measured under isothermal (i.e., pulsed) conditions at various temperatures, as reported in [39], where further details concerning the model and the underlying transistor physics can be found.

D. Electrothermal Analysis

The transistor subcircuit was connected to the NCTN presented in Section III; as a result, the whole device structure is translated into a macrocircuit describing both the electrical behavior and the nonlinear power-temperature feedback. The solution of the macrocircuit was performed with PSPICE, although any commercial SPICE-like simulator can in principle be employed; the studies conducted in [39] and [46] evidenced that exploiting the optimized PSPICE engine for linear problems favors low CPU time and memory requirements, as well as the absence of convergence issues.

The proposed approach was adopted to describe the dynamic ET behavior of the power MOSFET subject to a short-circuit test involving large power dissipation [39], [47]–[50]. In particular, from the time instant $t = 0$ s, the device was subject to $V_{GS} = 20$ V and $V_{DS} = 100$ V for 160 μs. Fig. 8 illustrates the transient evolution of drain current and temperature rise (averaged over the heat source) for the fully nonlinear case, for the linear counterpart, and for the latter corrected with the Kirchhoff's transformation with the 4H-SiC power factor applied to

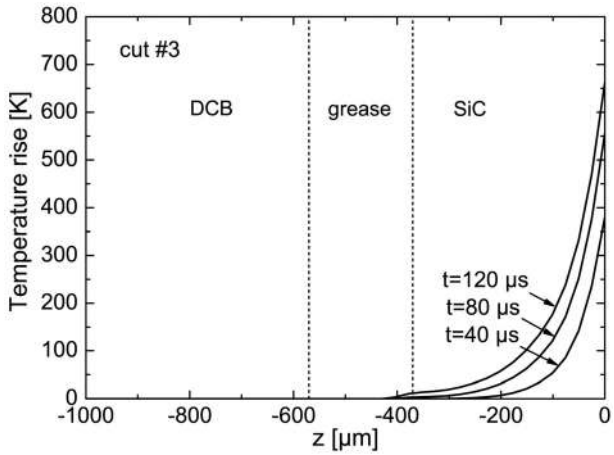

Fig. 10. Temperature rise profiles along the vertical cut #3 shown in Fig. 2 during the short-circuit test at $t = 40$, 80, and 120 μs, as computed in a post-processing step.

the whole macrocircuit (i.e., to the whole structure). The following comments are in order:

- the time elapsed by PSPICE was about 2 s for the linear/Kirchhoff's cases and 50 s for the nonlinear one, whereas several hours or even days would be needed by resorting to approaches based on numerical tools (e.g., [1]–[4]);
- for short times, the drain current rapidly grows due to the high PTC dictated by the NTC of the threshold voltage and the PTC of channel mobility;
- as the temperature reaches values at which the NTC of the mobility dominates over the other mechanisms, the current reduces;
- neglecting nonlinear thermal effects leads to a considerable overestimation of the current and underestimation of the temperature for medium/long times (i.e., medium/high temperatures);
- applying the Kirchhoff's transformation with the power factor of 4H-SiC enhances ET effects in comparison with the exact nonlinear case; it must be remarked that, for this specific analysis, the temperature overestimation for medium/long times, although considerable, is not dramatic due to the NTC of the drain current that alleviates the power-temperature feedback.

Figs. 9 and 10 depict the temperature rise profiles as computed in a 1-s-long postprocessing step at the operating points highlighted in Fig. 8(b). It must be remarked that the knowledge of the whole temperature distribution is important, since the value of the temperature peak, as well as its position, can be determined for further reliability considerations. As an example, it can be evaluated that the temperature rise peak along cut #1 at $t = 120$ μs in Fig. 9(a) is 18% higher than the average temperature rise over the active area shown in Fig. 8(b). Fig. 10 clarifies that during the short-circuit test the heat is still confined in the SiC die, not having reached the DCB yet.

VI. Conclusion

In this study, an approach has been proposed to perform nonlinear dynamic electrothermal analyses of power devices and systems using commercial SPICE-like circuit simulators. Compared to state-of-the-art alternative strategies, the method requires ultra short CPU time by preserving excellent accuracy over an extremely wide range of temperature, and does not need a calibration procedure relying on cumbersome measurements or 3-D numerical simulations of the thermal impedance. The transistors, modeled by behavioral subcircuits with temperature-varying physical parameters, are coupled to a nonlinear compact thermal network that describes the power-temperature feedback and accounts for the temperature dependence of the thermal conductivities of materials. Such a network is extracted from a finite-element discretization of the structure under analysis by a novel very fast MOR algorithm, and—unlike commonly employed methods—allows reconstructing the evolution of the temperature field in all points at each time instant of a thermal or electrothermal analysis. The approach has been exploited to effectively analyze the behavior of a packaged 1200-V 50-A 4H-SiC power MOSFET coping with harsh electrical/thermal conditions during a short-circuit test. The current and temperature waveforms have been simulated with PSPICE in less than 1 min on a normal PC. It has been found that disregarding nonlinear thermal effects or applying the widely used Kirchhoff's transformation leads to intolerable discrepancies with respect to the accurate solution obtained with the nonlinear network. The proposed approach can be therefore suggested to support the thermal design of power devices and systems destined to applications where significant temperatures are expected.

Appendix: Kirchhoff's Transformation

The most common approach to describing nonlinear heat diffusion problems with an NCTN exploits the Kirchhoff's transformation [19], [20]. In such an approach, the thermal parameters in the heat diffusion equation (1), (3) are assumed to take the form

$$k(\mathbf{r}, \vartheta(\mathbf{r},t)) = k(\mathbf{r},0)\, f(\vartheta(\mathbf{r},t)),$$
$$\rho(\mathbf{r}, \vartheta(\mathbf{r},t))c(\mathbf{r}, \vartheta(\mathbf{r},t)) = \rho(\mathbf{r},0)c(\mathbf{r},0)\, f(\vartheta(\mathbf{r},t)), \quad \text{(A1)}$$

$$h(\mathbf{r}, \vartheta(\mathbf{r},t)) = h(\mathbf{r},0) \int_0^{\vartheta(\mathbf{r},t)} f(\tau)\, d\tau \Big/ \vartheta(\mathbf{r},t) \quad \text{(A2)}$$

being $f(\cdot)$ a given positive function. In this case, by the change of variable

$$u(\mathbf{r},t) = \int_0^{\vartheta(\mathbf{r},t)} f(\tau)\, d\tau = F(\vartheta(\mathbf{r},t)) \quad \text{(A3)}$$

the nonlinear heat diffusion problem is mapped onto the linear heat diffusion equation

$$\rho(\mathbf{r},0)c(\mathbf{r},0)\frac{\partial u}{\partial t}(\mathbf{r},t) + \nabla \cdot [-k(\mathbf{r},0)\nabla u(\mathbf{r},t)] = q(\mathbf{r},t) \quad \text{(A4)}$$

with linear boundary conditions

$$-k(\mathbf{r},0)\frac{\partial u}{\partial n}(\mathbf{r},t) = h(\mathbf{r},0)u(\mathbf{r},t) \tag{A5}$$

and initial conditions

$$u(\mathbf{r},0) = 0. \tag{A6}$$

From the solution to this linear heat diffusion problem, the solution to the nonlinear one is simply achieved by inverting the Kirchhoff's transformation (A3). As a result, an NCTN modeling the nonlinear heat diffusion problem (1), (3) is obtained by determining a CTN modeling the linear heat diffusion problem (A4), (A5) by any suitable technique such as the MPMM algorithm [12], and inverting the Kirchhoff's transformation (A3).

However, when considering power electronics applications, the thermal conductivity of the materials is commonly assumed to depend on $\vartheta(\mathbf{r},t)$ according to (2) in which parameters $k_0(\mathbf{r})$ and $m(\mathbf{r})$ are material-dependent. Besides, the specific heat $c(\mathbf{r})$, the mass density $\rho(\mathbf{r})$, and the heat transfer coefficient $h(\mathbf{r})$ are commonly assumed to be temperature independent, and thus, do not vary according to (A1), (A2). In such a case, the Kirchhoff's transformation approach does *not* rigorously apply. An heuristic practice is to assume a spatially uniform temperature dependence for all material thermal parameters of the form (2) with m assumed independent of the position vector $\mathbf{r}$, and to apply the Kirchhoff's transformation approach. In this way, $f(\tau) = (1+\tau/T_0)^m$ so that the Kirchhoff's transformation is

$$u(\mathbf{r},t) = F(\vartheta(\mathbf{r},t)) = \frac{T_0}{m+1}\left[\left(1+\frac{\vartheta(\mathbf{r},t)}{T_0}\right)^{m+1} - 1\right]$$

and its inverse is

$$\vartheta(\mathbf{r},t) = T_0\left[\left(1+\tfrac{m+1}{T_0}\,u(\mathbf{r},t)\right)^{\frac{1}{m+1}} - 1\right]. \tag{A7}$$

As numerically shown in Section V, in many electronics applications, the Kirchhoff's transformation introduces large inaccuracies that cannot be controlled. For this reason, a rigorous, alternative strategy to dynamic compact thermal modeling of nonlinear heat diffusion is highly desired.

REFERENCES

[1] W. Van Petegem, B. Geeraerts, W. Sansen, and B. Graindourze, "Electrothermal simulation and design of integrated circuits," *IEEE J. Solid-State Circuits*, vol. 29, no. 2, pp. 143–146, Feb. 1994.

[2] S. Wünsche, C. Clauß, P. Schwarz, and F. Winkler, "Electro-thermal circuit simulation using simulator coupling," *IEEE Trans. VLSI Syst.*, vol. 5, no. 3, pp. 277–282, Sep. 1997.

[3] G. De Falco, M. Riccio, G. Breglio, and A. Irace, "Thermal-aware design and fault analysis of a DC/DC parallel resonant converter," *Microelectron. Reliab.*, vol. 54, no. 9–10, pp. 1833–1838, 2014.

[4] V. Košel, S. de Filippis, L. Chen, S. Decker, and A. Irace, "FEM simulation approach to investigate electro-thermal behavior of power transistors in 3-D," *Microelectron. Reliab.*, vol. 53, no. 3, pp. 356–362, 2013.

[5] K. Fukahori and P. R. Gray, "Computer simulation of integrated circuits in the presence of electro-thermal interaction," *IEEE J. Solid-State Circuits*, vol. 11, no. 12, pp. 834–846, Dec. 1976.

[6] A. R. Hefner and D. L. Blackburn, "Simulating the dynamic electrothermal behavior of power electronic circuits and systems," *IEEE Trans. Power Electron.*, vol. 8, no. 4, pp. 376–385, Oct. 1993.

[7] S.–S. Lee and D. J. Allstot, "Electrothermal simulation of integrated circuits," *IEEE J. Solid-State Circuits*, vol. 28, no. 12, pp. 1283–1293, Dec. 1993.

[8] B. H. Krabbenborg, A. Bosma, H. C. de Graaff, and A. J. Mouthaan, "Layout to circuit extraction for three-dimensional thermal-electrical circuit simulations of device structures," *IEEE Trans. Comput.-Aided Des. Integr. Circuits Syst.*, vol. 15, no. 7, pp. 765–774, Jul. 1996.

[9] J. Tzer Hsu and L. Vu-Quoc, "A rational formulation of thermal circuit models for electrothermal simulation. I. Finite element method," *IEEE Trans. Circuits Syst. I*, vol. 43, no. 9, pp. 721–732, Sep. 1996.

[10] G. Digele, S. Lindenkreuz, and E. Kasper, "Fully coupled dynamic electrothermal simulation," *IEEE Trans. VLSI Syst.*, vol. 5, no. 3, pp. 250–257, Sep. 1997.

[11] L. Codecasa, D. D'Amore, and P. Maffezzoni, "An Arnoldi based thermal network reduction method for electro-thermal analysis," *IEEE Trans. Compon. Packag. Technol.*, vol. 26, no. 1, pp. 186–192, Mar. 2003.

[12] L. Codecasa, D. D'Amore, and P. Maffezzoni, "Compact modeling of electrical devices for electrothermal analysis," *IEEE Trans. Circuits Syst. I*, vol. 50, no. 4, pp. 465–476, Apr. 2003.

[13] P. E. Bagnoli, C. Casarosa, M. Ciampi, and E. Dallago, "Thermal resistance analysis by induced transient (TRAIT) method for power electronic devices thermal characterization–Part I: Fundamentals and theory," *IEEE Trans. Power Electron.*, vol. 13, no. 6, pp. 1208–1219, Nov. 1998.

[14] P. E. Bagnoli, C. Casarosa, E. Dallago, and M. Nardoni, "Thermal resistance analysis by induced transient (TRAIT) method for power electronic devices thermal characterization–Part II: Practice and experiments," *IEEE Trans. Power Electron.*, vol. 13, no. 6, pp. 1220–1228, Nov. 1998.

[15] L. Codecasa, D. D'Amore, and P. Maffezzoni, "Compact thermal networks for modeling packages," *IEEE Trans. Compon. Packag. Technol.*, vol. 27, no. 1, pp. 96–103, Mar. 2004.

[16] L. Codecasa, "Compact models of dynamic thermal networks with many heat sources," *IEEE Trans. Compon. Packag. Technol.*, vol. 30, no. 4, pp. 653–659, Dec. 2007.

[17] P. L. Evans, A. Castellazzi, and C. M. Johnson, "Automated fast extraction of compact thermal models for power electronic modules," *IEEE Trans. Power Electron.*, vol. 28, no. 10, pp. 4791–4802, Oct. 2013.

[18] M. Rencz and V. Székely, "Studies on the nonlinearity effects in dynamic compact model generation of packages," *IEEE Trans. Compon. Packag. Technol.*, vol. 27, no. 1, pp. 124–130, Mar. 2004.

[19] H. S. Carlslaw and J. C. Jaeger, *Conduction of Heat in Solids*, 2nd ed. London, U.K.: Oxford Univ. Press, 1959, sec. I.1.6.

[20] M. N. Özişik, *Boundary Value Problems of Heat Conduction*. New York, NY, USA: Dover, 1989, sec. 8.2.

[21] L. Codecasa, V. d'Alessandro, A. Magnani, and N. Rinaldi, "Compact dynamic modeling for fast simulation of nonlinear heat conduction in ultra-thin chip stacking technology," *IEEE Trans. Compon. Packag. Manuf. Technol.*, vol. 4, no. 11, pp. 1785–1795, Nov. 2014.

[22] M. Pfost, C. Boianceanu, H. Lohmeyer, and M. Stecher, "Electrothermal simulation of self-heating in DMOS transistors up to thermal runaway," *IEEE Trans. Electron Devices*, vol. 60, no. 2, pp. 699–707, Feb. 2013.

[23] A. Chvála, D. Donoval, J. Marek, P. Príbytný, M. Molnár, and M. Mikolášek, "Fast 3-D electrothermal device/circuit simulation of power superjunction MOSFET based on SDevice and HSPICE interaction," *IEEE Trans. Electron Devices*, vol. 61, no. 4, pp. 1116–1122, Apr. 2014.

[24] K. Górecki and J. Zarębski, "Nonlinear compact thermal model of power semiconductor devices," *IEEE Trans. Compon. Packag. Technol.*, vol. 33, no. 3, pp. 643–647, Sep. 2010.

[25] J. Marek, A. Chvála, D. Donoval, P. Príbytný, M. Molnár, and M. Mikolášek, "Compact model of power MOSFET with temperature dependent Cauer RC network for more accurate thermal simulations," *Solid-State Electron.*, vol. 94, pp. 44–50, 2014.

[26] A. K. Sahoo, S. Frégonèse, R. Desposito, K. Aufinger, C. Maneux, and T. Zimmer, "A geometry scalable model for nonlinear thermal impedance of trench isolated HBTs," *IEEE Electron Device Lett.*, vol. 36, no. 1, pp. 56–58, Jan. 2015.

[27] M. Cotorogea, "Using analog behavioral modeling in PSpice for the implementation of subcircuit-models of power devices," in *Proc. IEEE Int. Power Electron. Congr.*, 1998, pp. 158–163.

[28] W. J. Rugh, *Nonlinear System Theory: The Volterra's-Wiener Approach*. Baltimore, MD, USA: Johns Hopkins Univ. Press, 1981.

[29] Y. Notay, "An aggregation-based algebraic multigrid method," *Electron. Trans. Numer. Anal.*, vol. 37, pp. 123–146, 2011.

[30] (2011). [Online]. Available: http://www.cree.com/Power/Products/MOSFETs/Bare-die/CPMF-1200-S080B

[31] X. Zhong, X. Wu, W. Zhou, and K. Sheng, "An all-SiC high-frequency boost DC-DC converter operating at 320 °C junction temperature," *IEEE Trans. Power Electron.*, vol. 29, no. 10, pp. 5091–5096, Oct. 2014.

[32] M. Östling, R. Ghandi, and C.-M. Zetterling, "SiC power devices–present status, applications and future perspective," in *Proc. IEEE Int. Symp. Power Semicond. Devices*, 2011, pp. 10–15.

[33] Comsol Multiphysics 3.5a, *User's Manual*, COMSOL AB, Stockholm, Sweden, 2008.

[34] Y. Goldberg, M. E. Levinshtein, and S. L. Rumyantsev *Properties of Advanced Semiconductor Materials: GaN, AlN, InN, BN, SiC, SiGe*, M. E. Levinshtein, S. L. Rumyantsev, and M. S. Shur, Eds. New York, NY, USA: John Wiley & Sons, Inc., 2001.

[35] R. P. Joshi, P. G. Neudeck, and C. Fazi, "Analysis of the temperature dependent thermal conductivity of silicon carbide for high temperature applications," *J. Appl. Phys.*, vol. 88, no. 1, pp. 265–269, 2000.

[36] J. H. Lienhard IV and J. H. Lienhard V, *A Heat Transfer Textbook*, 3rd ed. Cambridge, MA, USA: Phlogiston Press, 2008.

[37] V. Palankovski and R. Quay, *Analysis and Simulation of Heterostructure Devices*. New York, NY, USA: Springer Verlag, 2004.

[38] PSPICE, *User's Manual*, "Cadence Design Systems, Inc. (Cadence), Seely Ave, San Jose, CA, USA".

[39] V. d'Alessandro, A. Magnani, M. Riccio, G. Breglio, A. Irace, N. Rinaldi, and A. Castellazzi, "SPICE modeling and dynamic electrothermal simulation of SiC power MOSFETs," in *Proc. IEEE Int. Symp. Power Semicond. Devices*, 2014, pp. 285–288.

[40] H. Ö. Ólafsson, G. Gudjónsson, F. Allerstam, E. Ö. Sveinbjörnsson, T. Rödle, and R. Jos, "Stable operation of high mobility 4H-SiC MOSFETs at elevated temperatures," *Electron. Lett.*, vol. 41, no. 14, pp. 825–826, 2005.

[41] J. Wang, T. Zhao, J. Li, A. Q. Huang, R. Callanan, F. Husna, and A. Agarwal, "Characterization, modeling, and application of 10-kV SiC MOSFET," *IEEE Trans. Electron Devices*, vol. 55, no. 8, pp. 1798–1806, Aug. 2008.

[42] S. Chen, C. Cai, T. Wang, Q. Guo, and K. Sheng, "Cryogenic and high temperature performance of 4H-SiC power MOSFETs," in *Proc. IEEE Appl. Power Electron. Conf.*, 2013, pp. 207–210.

[43] A. Pérez-Tomás, P. Brosselard, P. Godignon, J. Millán, N. Mestres, M. Jennings, J. A. Covington, and P. A. Mawby, "Field-effect mobility temperature modeling of 4H-SiC metal-oxide-semiconductor transistors," *J. Appl. Phys.*, vol. 100, no. 11, pp. 114508-1–114508-6, 2006.

[44] L. Cheng, A. K. Agarwal, S. Dhar, S.-H. Ryu, and J. W. Palmour, "Static performance of 20 A, 1200 V 4H-SiC power MOSFETs at temperatures of −187 °C to 300 °C," *J. Electonic Mater.*, vol. 41, no. 5, pp. 910–914, 2012.

[45] X. Huang, G. Wang, Y. Li, A. Q. Huang, and B. Baliga, "Short-circuit capability of 1200 V SiC MOSFET and JFET for fault protection," in *Proc. IEEE Appl. Power Electron. Conf.*, 2013, pp. 197–200.

[46] V. d'Alessandro, A. Magnani, M. Riccio, Y. Iwahashi, G. Breglio, N. Rinaldi, and A. Irace, "Analysis of the UIS behavior of power devices by means of SPICE-based electrothermal simulations," *Microelectron. Reliab.*, vol. 53, no. 9–11, pp. 1713–1718, 2013.

[47] A. Castellazzi, T. Funaki, T. Kimoto, and T. Hikihara, "Thermal instability effects in SiC power MOSFETs," *Microelectron. Reliab.*, vol. 52, no. 9–10, pp. 2414–2419, 2012.

[48] T.-T. Nguyen, A. Ahmed, T. V. Thang, and J.-H. Park, "Gate oxide reliability issues of SiC MOSFETs under short-circuit operation," *IEEE Trans. Power Electron.*, vol. 30, no. 5, pp. 2445–2455, May 2015.

[49] G. Romano, L. Maresca, M. Riccio, V. d'Alessandro, G. Breglio, A. Irace, A. Fayyaz, and A. Castellazzi, "Short-circuit failure mechanism of SiC power MOSFETs," in *Proc. IEEE Int. Symp. Power Semicond. Devices*, 2015, pp. 345–348.

[50] Z. Wang, X. Shi, L. Tolbert, F. Wang, Z. Liang, D. Costinett, and B. J. Blalock, "Temperature dependent short circuit capability of Silicon Carbide (SiC) power MOSFETs," *IEEE Trans. Power Electron.*, vol. 31, no. 2, pp. 1555–1566, Feb. 2016.